Evaluation of Particle Size and Particle Shape Distributions in Al-Al_3Ni FGMs Fabricated by a Centrifugal *in-situ* Method

Yoshimi Watanabe*, Ryuho Sato, Koichi Matsuda
Department of Functional Machinery and Mechanics, Shinshu University
3-15-1 Tokida, Ueda 386-8567, Japan
and
Yasuyoshi Fukui
Department of Mechanical Engineering, Kagoshima University
1-21-40 Korimoto, Kagoshima 890-0065, Japan

ABSTRACT

This paper reports on the variation of particle size, particle shape and volume fraction distributions in Al-Al_3Ni functionally graded materials (FGMs) fabricated by a centrifugal *in-situ* method. Eight specimens of Al-Al_3Ni FGM were systematically selected for the experimental analysis. The microstructures of Al_3Ni primary crystal particles were observed and then gradients of volume fraction of Al_3Ni particles towards centrifugal force direction were measured. A detailed evaluation of particle size was done considering the area-equivalent diameter from cross-sectional area of each Al_3Ni particle. Moreover, particle shape distributions were also conducted using functions concerning with both fractal dimension and circularity of particles. It is revealed that both particle size and particle shape of Al_3Ni had graded distributions as well as volume fraction distributions within the FGMs. Those results were explained considering the effect of applied G number, Ni content in Al-Ni master alloy, cooling rate and stirring of melt.

Key words: Functionally graded materials (FGMs), Al-Al_3Ni, centrifugal *in-situ* method, particle size, particle shape, cooling rate, fractal dimension, circularity, stirring

1. INTRODUCTION

Functionally graded material (FGM) belongs to a relatively new class of inhomogeneous composite materials, which consists of more than two different materials with gradient composition /1, 2/. The design of composition results in gradients of physical and chemical properties. Many processing methods have been used to fabricate FGMs /1, 2/, and one of the FGM fabrication methods is the centrifugal method proposed by Fukui *et al.* /3-5/. It has been shown that metal base intermetallic compound-dispersed FGMs can be successfully fabricated by the centrifugal method /5/. The formation of composition gradient depends mainly on the applied G number (ratio of centrifugal force to gravity). In case of metal intermetallic compound FGMs, the process can be classified into two categories depending on the operating temperature. If the liquidus temperature of the master alloy is higher than the processing temperature as shown in Figure 1 (a), the intermetallic compound written as A_mB in Figure 1 remains solid in a liquid matrix during the centrifugal casting. The situation is similar to a fabrication of metal base ceramic particles dispersed FGMs /6/, and the method is referred to as a centrifugal solid-particle method /7, 8/. On the other hand, if the liquidus temperature of the master alloy is lower than the

* Corresponding author. E-mail address: yoshimi@giptc.shinshu-u.ac.jp

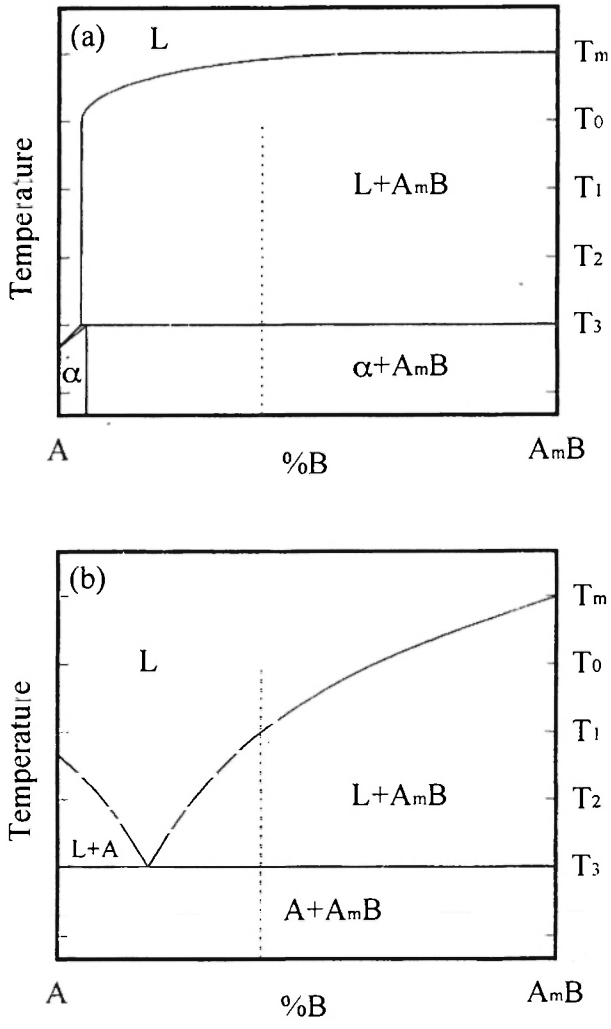

Fig. 1: Two types of phase diagrams. (a); Applicable to a centrifugal solid-particle method. (b); Applicable to a centrifugal *in-situ* method.

processing temperature as shown in Figure 1 (b), centrifugal force is applied during the solidification both of the intermetallic compound, A_mB, and the matrix. The process is similar to a production of *in-situ* composite using the crystallization phenomena /9/ and is referred to as a centrifugal *in-situ* method /10-12/.

It is well known that the particle size and particle shape in particle-reinforced or dispersion-strengthened composite material play an important role in achieving superior mechanical properties. Therefore, a detailed knowledge of both particle size and particle shape distributions in the FGMs is also required to predict and/or obtain the better mechanical properties. In the case of FGM made by the centrifugal *in-situ* method, the centrifugal force is applied to a completely liquid phase and the intermetallic compound particles crystallize from the liquid phase directly during casting. Both size and shape of the crystallized particles in the FGMs should be affected by the solidification process under the centrifugal force. Those parameters are applied G number, composition of master alloy, cooling rate, *etc.* It would be useful to obtain information about particle size and particle shape distributions in the FGMs fabricated by the centrifugal *in-situ* method from the viewpoint of both a fundamental understanding and a technological application.

In the present study, ring-shaped and cylindrical Al-Al_3Ni FGMs are systematically fabricated by the centrifugal *in-situ* method from two kinds of Al-Ni master alloys. The microstructures of Al_3Ni particles are observed with an optical microscope, and the composition gradients within the FGMs were studied. Moreover, particle size and particle shape distributions are determined by calculating the parameters concerning with the size and shape of each. Based on the observations, the origin of the gradients formation in the FGMs is discussed.

2. EVALUATION OF PARTICLE SHAPE

In order to describe the particle shape distributions in Al-Al_3Ni FGMs quantitatively, the following two methods are adopted. One is a box-counting method using fractal dimension, D, which is given by the following equation /13/:

$$N(r) = kr^{-D} \tag{1}$$

where $N(r)$ is number of divided square, k is a constant and r is a size of square boxes. Figure 2 shows a schematic illustration of the box-counting method. The fractal dimension takes a larger value for a complex-shaped particle. The other is circularity, F, which is given by the following equation:

$$F = 4\pi S / L^2 \tag{2}$$

where L is perimeter length of the particle and S is the area of the cross-section of the particle. The circularity

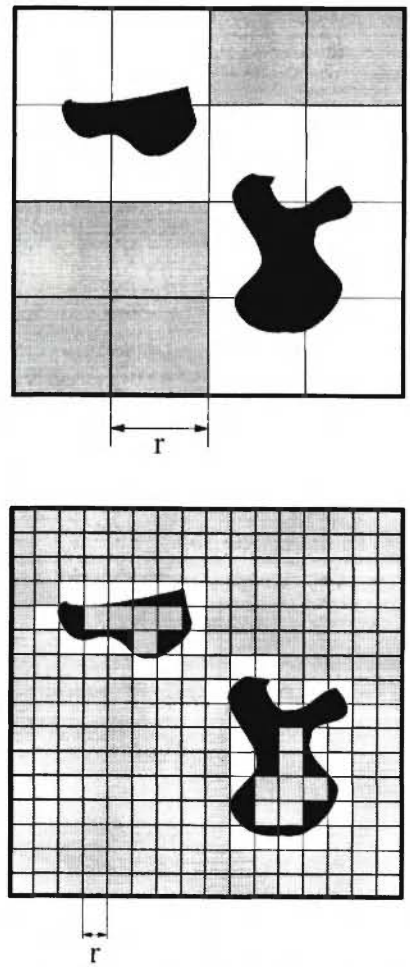

Fig. 2: Schematic illustration of the box-counting method applied to the estimation of fractal dimension, D.

ranges between the values $F = 0$ and $F = 1$, and it becomes 1 for a perfect circle. The fractal dimension and circularity values of some typical shapes are shown in Figure 3. A complex shape has a larger fractal dimension, and circularity value becomes smaller when the aspect ratio becomes small.

3. EXPERIMENTAL

In this study, eight Al-Al_3Ni FGM specimens, termed specimens R1~R7 and C1, were systematically fabricated by the centrifugal *in-situ* method. The casting conditions applied in the present study and notations of the specimens are summarized in Table 1. These came from the combination of master ingots, applied G number and specimen shape considering the convenience of analysis. The ingots were Al-13 mass% Ni and 20 mass% Ni alloys and both liquidus temperatures for the Al_3Ni primary crystal were lower than the processing temperatures (see Figure 4 /14/) for specimens R1~R7. The applied G numbers were 30, 50 and 80 and the centrifugal force was applied during the solidification of the Al_3Ni intermetallic compound and Al matrix. The specimen shapes were rings of 90mm outer diameter and roughly 25mm wall thickness and cylinder of 30mm length. The outlines of the apparatuses for the fabrication of the ring-shaped and cylinder FGMs are shown in Figures 5 (a) and (b). The

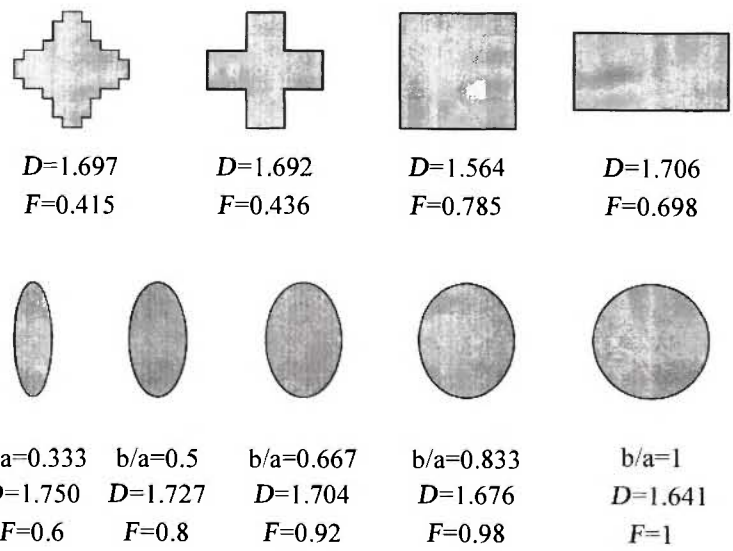

Fig. 3: The fractal dimension and circularity values of some typical shapes.

Table 1
Casting conditions and notations of the specimens.

	Initial master ingot	Pouring temp.	Mold temp.	*G* number/ Cooling rate	Shape	Temp. gradient
Specimen R1	13mass% Ni	900 °C	600 °C	30 / 0.27 °C/s	Ring	Large
Specimen R2	13mass% Ni	900 °C	600 °C	50 / 0.29 °C/s	Ring	Large
Specimen R3	13mass% Ni	900 °C	600 °C	80 / 0.37 °C/s	Ring	Large
Specimen R4	20mass% Ni	900 °C	600 °C	30 / 0.27 °C/s	Ring	Large
Specimen R5	20mass% Ni	900 °C	600 °C	50 / 0.29 °C/s	Ring	Large
Specimen R6	20mass% Ni	900 °C	600 °C	80 / 0.37 °C/s	Ring	Large
Specimen R7	20mass% Ni	900 °C	600 °C	50 /0.056 °C/s	Ring	Small
Specimen C1	20mass% Ni	-------	730 °C	50 /~0.05 °C/s	Cylinder	Small

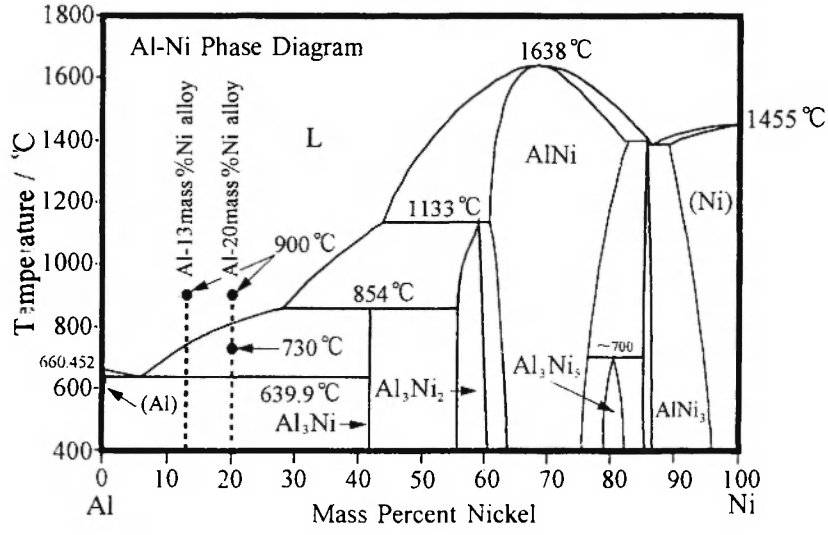

Fig. 4: Al-Ni phase diagram after Massalski /14/.

difference in cooling rate between specimens R1~R6 and specimens R7 and C1 was achieved by the melt solidified out of and in the mold-heating furnace. In the former case, the mold-heating furnace is removed after the casting and the mold is cooled in air until complete solidification occurs /5/. It must be emphasized here that in the case of specimen C1, the processing temperature was lower than liquidus temperature for the Al_3Ni primary crystal, as shown in Fig. 4. As can be seen, half the volume fraction of the Al_3Ni primary crystal remains solid in a liquid matrix during the centrifugal method, and this situation is similar to the centrifugal solid-particle method. However, the volume fraction of Al_3Ni primary crystal particles increases with cooling, and this phenomenon is similar to the centrifugal *in-situ* method. Thus, the fabrication method of specimen C1 belongs both to the centrifugal solid-particle and *in-situ* methods.

Each specimen was divided into ten regions of equal width along the centrifugal force direction, as shown in Figure 5, for the evaluation of the character as a function of position normalized with radial thickness of

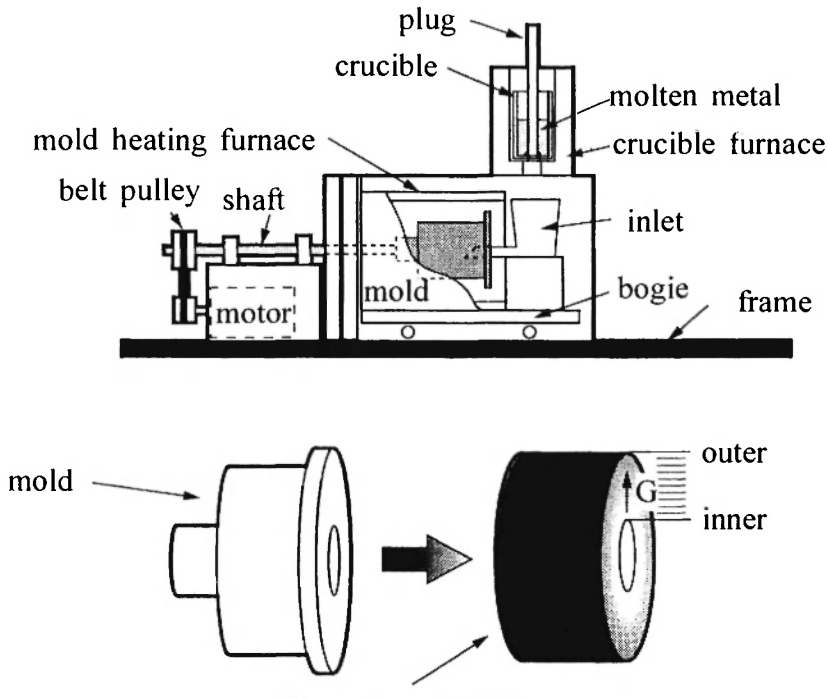

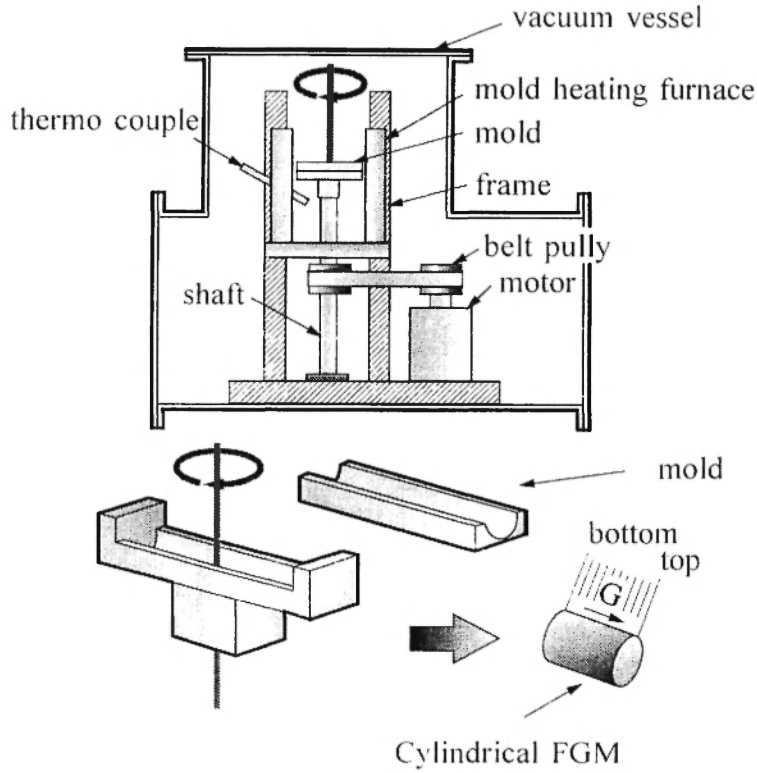

Fig. 5: The apparatuses for the centrifugal *in-situ* method performed in this study. (a): cylindrical FGM and (b): ring-shaped FGM.

ring or distance (*i.e.*, height) of cylinder. Hereafter they are referred to as normalized position and 0.0 and 1.0 of normalized position are inside and outside surface of peripheral position, respectively. The volume fraction, particle size, fractal dimension and circularity of Al_3Ni particles in each region were measured by optical microscopy of metallographic samples prepared by standard metallographic polishing techniques. Microscopic observation was easily done without any etching because the color of Al_3Ni phase and Al matrix is clearly different and is black and gray, respectively.

A supplemental experiment to reveal the stir effect on the Al_3Ni particle shape was also carried out. The Al-20 mass %Ni alloy was melted under air gas atmosphere in a steel mold. Then, this melt was cooled down to 530°C in the furnace, and subsequently water quenched. At the same time, this melt was stirred with steel rotor immersed in it at the rates of 250 rpm and 500 rpm until the melt reached 590 °C. The rotor has two rectangular fins of 15 mm x 55 mm x 3 mm in size. Both the steel mold and steel rotor were coated with heatproof paint in order to avoid erosion by the melt. Microscopic observations were also done.

4. RESULTS

4.1 Microstructures of Al-Al_3Ni FGMs fabricated by the centrifugal *in-situ* method

Figure 6 shows typical microstructures of the ring-shaped specimen R5. Figures 6 (a), (b) and (c) are taken at inner, interior and outer peripheral regions of the ring, respectively. Microstructures of the cylindrical specimen C1 are shown in Figures 7 (a), (b) and (c), which are taken at bottom (inner peripheral), intermediate and top (outer peripheral) regions of the cylinder, respectively. It is found by quantitative energy dispersive X-ray (EDX) analysis that the black particles in Figures 6 and 7 are stoichiometric Al_3Ni intermetallic compound and gray region is the Al matrix. It is apparent that the volume fraction of Al_3Ni primary crystals has graded distribution in each specimen. It is important to note here that the particle size of Al_3Ni primary crystal particles varies depending on the position. Moreover, in the case of specimen C1, particle shape of Al_3Ni primary crystal particles changes from place to place. Namely, granular and ellipsoidal particles are observed around the bottom and top

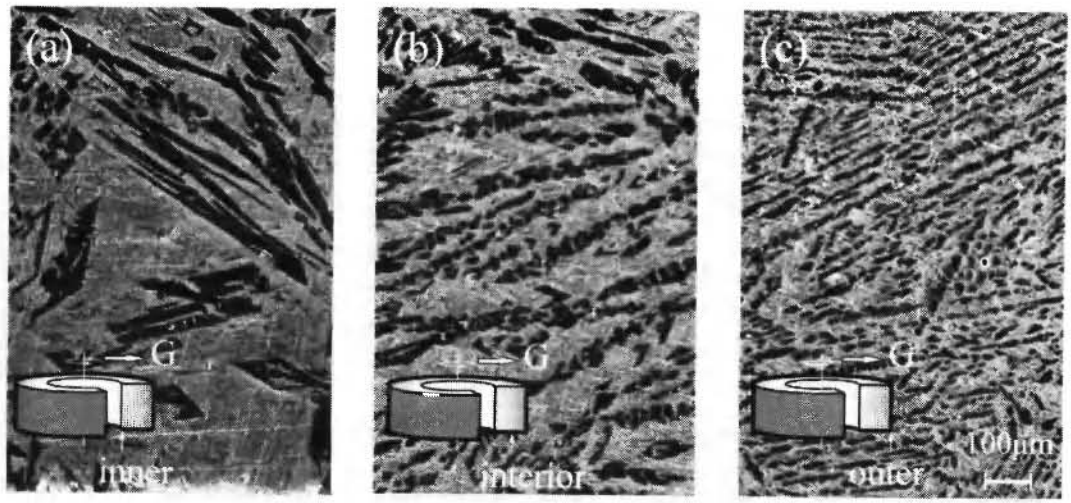

Fig. 6: Typical microstructures of the ring-shaped specimen R5. Initial master ingot was Al-20 mass% Ni, and applied G number was 50. (a), (b) and (c) are taken at the outer, the interior, and the inner regions of the ring, respectively.

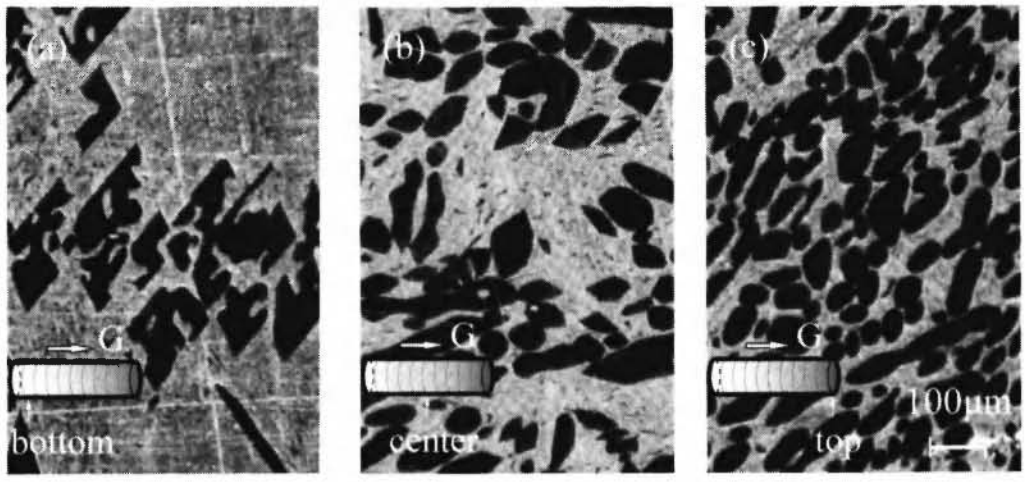

Fig. 7: Typical microstructures of the cylindrical specimen C1. (a), (b) and (c) are taken at the bottom, center and top regions of cylinder, respectively.

positions, respectively. These phenomena will be described more precisely in the next three sections.

4.2 Volume fraction distributions within the FGMs

The volume fraction of Al_3Ni particles in each of the ten-divided regions of the FGM specimen is measured, and the obtained distribution profiles of Al_3Ni particles are summarized in Figure 8. It reveals a tendency that the volume fraction of the Al_3Ni primary crystal particles increases towards the outer periphery that is the greater centrifugal force direction. Thus, both ring-shaped and cylindrical Al-Al_3Ni FGMs can be successfully fabricated by a centrifugal *in-situ* method. The relatively steeper distribution profiles of the Al_3Ni primary crystal particles are formed in the larger G number specimens as comparisons among specimens R1~R3 or specimens R4~R6. These results are in good agreement with a previous study /15/. Moreover, the specimens R1~R3 have steeper graded volume fraction compared with specimens R4~R6. The difference is well correlated with that of viscosity of the melt as follows. It is known that the viscosity of the melt increases according to the increase in volume fraction the suspension. The initial master ingots of specimens R1~R3 and R4~R6 are Al-13 mass% Ni and 20 mass% Ni alloys, respectively. Thus, the specimens R4~R6 show larger viscosity and this prevents the formation of volume fractional gradients.

It is noteworthy that the gradations of Al_3Ni particle distributions in the specimen R7 and particularly in the specimen C1 are greater than that in the specimen R5, even if the applied G number is the same. The difference is the cooling rate and that of the specimens R7 and C1 is much slower than in the case of specimen R5 (Table 1). Then the cooling rate may play an important role to control the volume fraction gradient in the FGMs.

Some words should be added regarding the mean volume fractions of primary particles in the specimens. The mean volume fractions of Al_3Ni for specimens R7 and C1 calculated from Figure 8 are 28 and 30 vol%, respectively. The values are much larger than that of specimen R5 (*i.e.*, 23 vol% Al_3Ni). Since the initial Al-20mass% Ni alloy contains 37vol% Al_3Ni phase including the fine Al_3Ni phase in eutectic structure (*i.e.*, 11 vol% Al_3Ni), theoretical volume fraction of primary Al_3Ni particle in these specimens is 26 vol%. For the specimen R5, the less observed value compared with theory should be attributed to the existence of the supersaturated solute Ni atoms in the matrix, which was

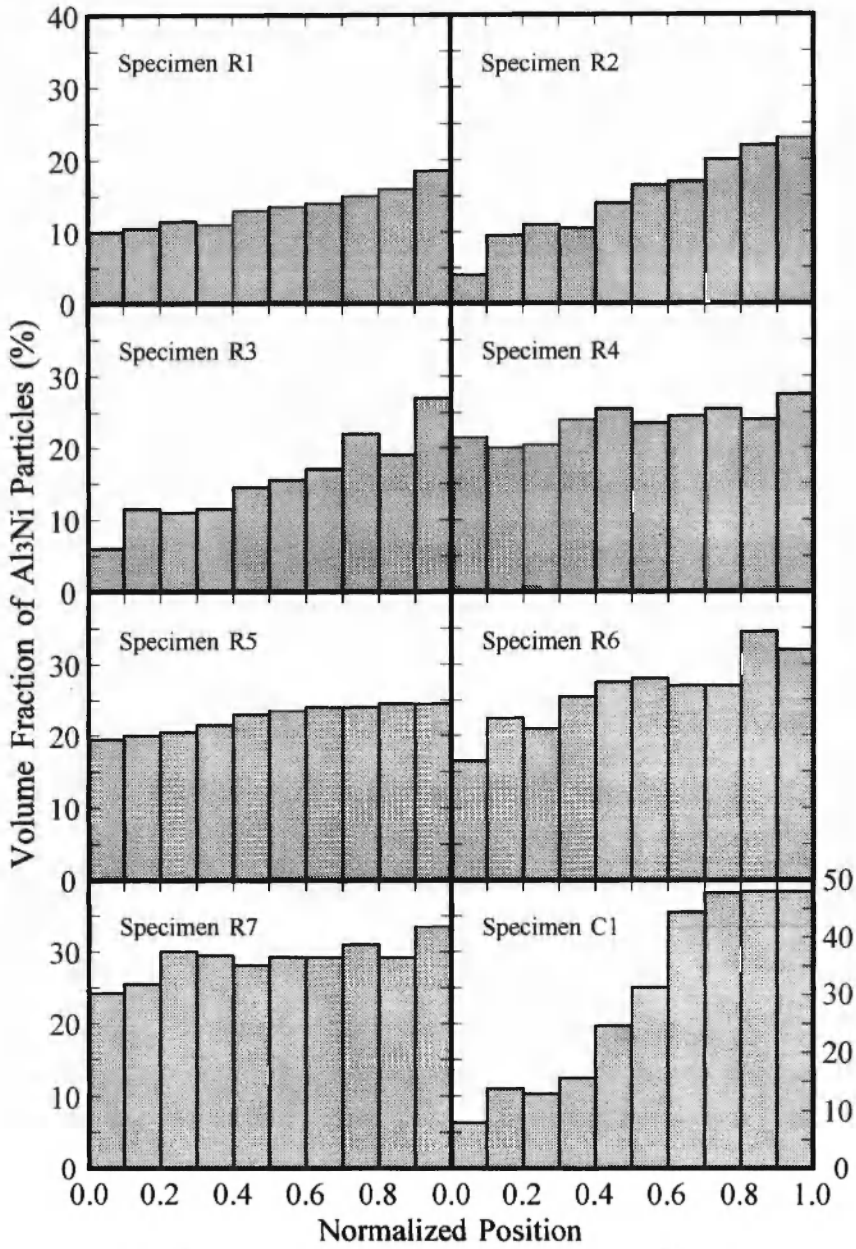

Fig. 8: The distributions of Al_3Ni primary crystal particles in the specimens. The abscissa represents the position in the centrifugal force direction, normalized by the wall thickness or cylinder length. 0.0 and 1.0 correspond to the inner and outer peripheries, respectively, for specimens R1-R7, and 0.0 and 1.0 correspond to the bottom and top surfaces of cylinder, respectively, for specimen C1.

caused by relatively high cooling rate. The cooling rate of 0.29 °C/s should be insufficient for the formation of the primary Al_3Ni particles. On the other hand, the origin greater than the theoretical value in the specimens R7 and C1 should be attributed to the Ostwald ripening, coarsening of primary particles by the dissolution of fine particles, during the slow cooling.

4.3 Particle size distributions within the FGMs

The Al_3Ni primary crystal particle size is investigated assuming the shape is spherical for the convenience of analysis. As can be seen, the shapes of Al_3Ni particles in Figures 6 and 7 are granular or ellipsoid. Thus the sizes are initially evaluated by

diameter from measured area of each Al_3Ni primary crystal particle. The typical result in the case of specimen R5 is shown in Figure 9. A tendency is observed for the average of particle size at the outer peripheral position to be smaller than that of the inner position. Based on the measurement of two-dimensional diameter, the average three-dimensional diameter which is given as the average two-dimensional diameter multiplied by $4\pi/16$/ is introduced for the evaluation of the size of Al_3Ni particles. Figure 10 shows the variation of the average three-dimensional diameter of Al_3Ni primary crystal particles as a function of normalized position. Figure 10 indicates that the present Al-Al_3Ni FGMs contains a graded distribution of the particle-size as well as the volume fraction. The average three-dimensional diameter in specimens R1~R6 shows a gradually decreased with increase of normalized position. The inclination for specimens R7 and C1 which are fabricated under relatively slow cooling rate is smaller than that for specimen R5. Moreover, it is apparent that the larger G number and the less Ni content in the master alloys give a smaller average particle size. Thus, in summary, the larger the applied G number, the less the Ni content in the master alloys and/or faster cooling rate show the tendency of a smaller average particle size which is obvious especially at the outer peripheral position. The origin of particle size distributions within the FGMs will be discussed later.

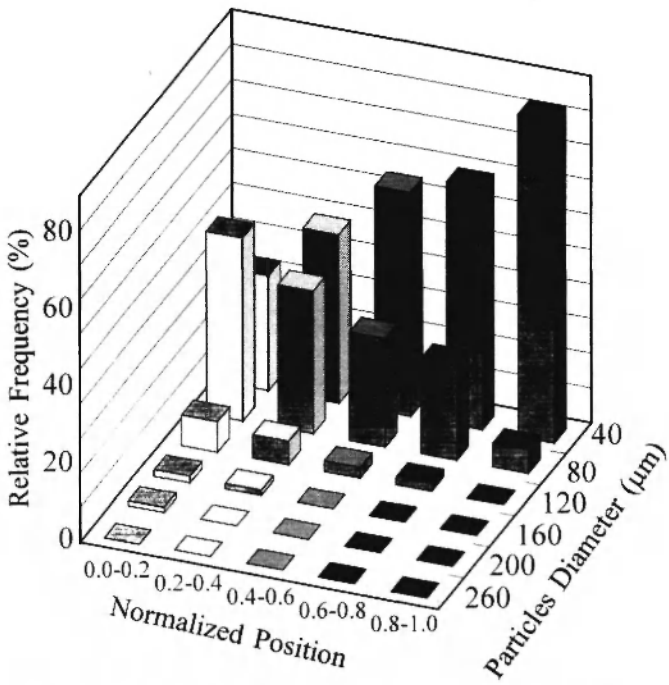

Fig. 9: The distribution of the area-equivalent diameter of Al_3Ni primary crystal particles at each region in the specimen R5.

4.4 Evaluation of particle shape

In the following, we will focus our attention on the particle shape. Fractal dimension and circularity distributions in the specimens R5 (representative of ring-shaped FGMs fabricated under rapid cooling rate), R7 (ring-shaped FGM fabricated under slow cooling rate), and C1 (cylindrical FGM fabricated under slow cooling rate) are calculated for the evaluation of the particle shape distributions in Al_3Ni FGMs quantitatively. Figure 11 shows the fractal dimension distributions of the Al_3Ni particles from Equation (1). The inclination of variation of fractal dimension is greater in the case of specimen C1. The tendency is easily understood from the comparison between Figures 6 and 7, because more complex shaped particles are found around the bottom position and simple shaped particles are formed around the top position in Figure 7. A similar fractal dimension distribution was evidenced in the recent study of Al-Al_3Ni FGMs fabricated by a semisolid forming /17/.

Circularity distributions of the Al_3Ni particles from Equation (2) are shown in Figure 12. It can be seen that the cylindrical specimen C1 has a circularity gradient while there are no gradients of circularity within the ring-shaped specimens R5 and R7. The fact that the circularity of specimen C1 increases with increasing the normalized position indicates that the rounder particles are formed around the top position (Fig. 7 (c)). That corresponds to the result that granular and ellipsoidal particles are observed around the bottom and top positions, respectively. This is different from ring specimens as shown in Fig. 6. Note that the clearer distributions are found in Figure 12. For this reason, the circularity is the better method to evaluate the particle shape distributions in the Al-Al_3Ni FGMs. The origin of particle shape distribution within the specimen C1 will also be discussed later.

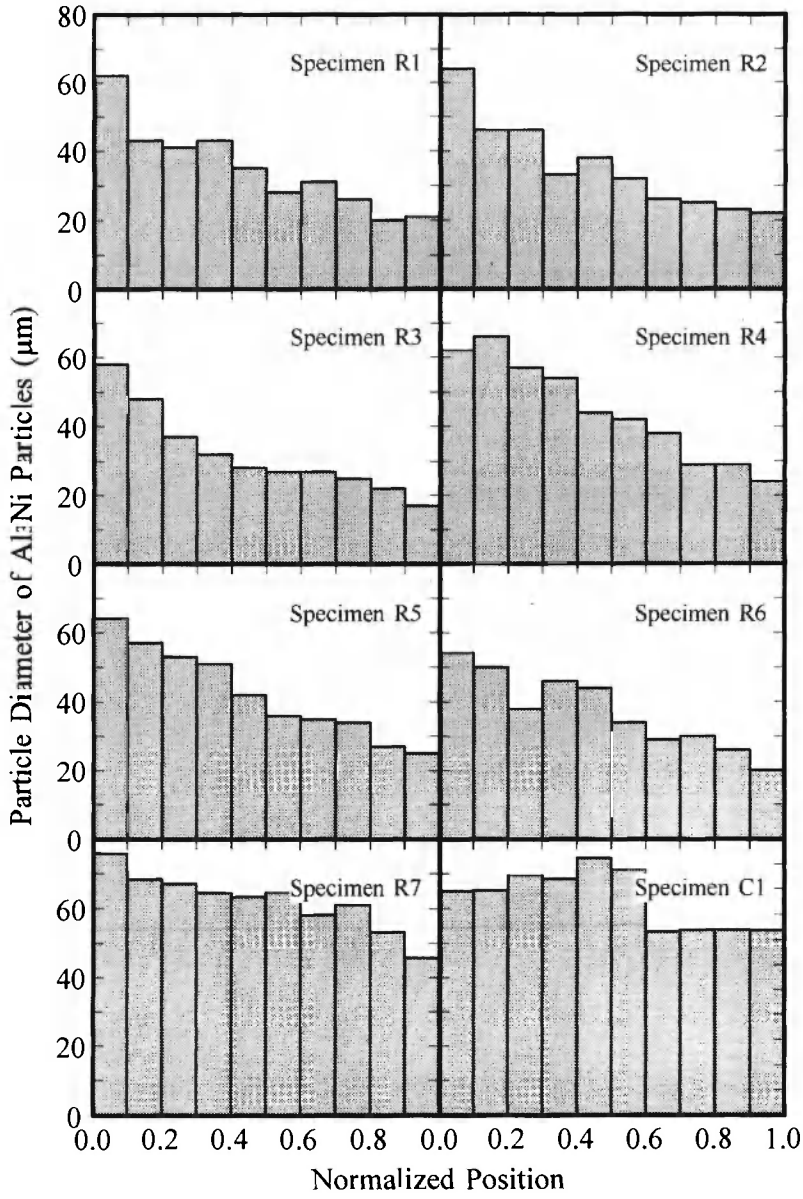

Fig. 10: The average three-dimensional diameter of Al_3Ni primary crystal particles in the specimens as a function of position.

5. DISCUSSION

5. 1 Origin of particle size gradient

It is found that the average three-dimensional diameter is distributed in the specimens R1~R6 in a gradually graded manner as shown in Figure 8, and the average particle size at the outer peripheral is smaller than that at the inner peripheral. The origin of particle size distributions within the ring-shaped FGMs is discussed as follows.

As a first consideration, the motion of solid particles in a viscous liquid under centrifugal force is focused. The motion obeys Stokes' law and the average particle size varies gradually depending on the radial position in the FGMs fabricated by the centrifugal solid-particle method /8/. If the density of larger particles is equal to

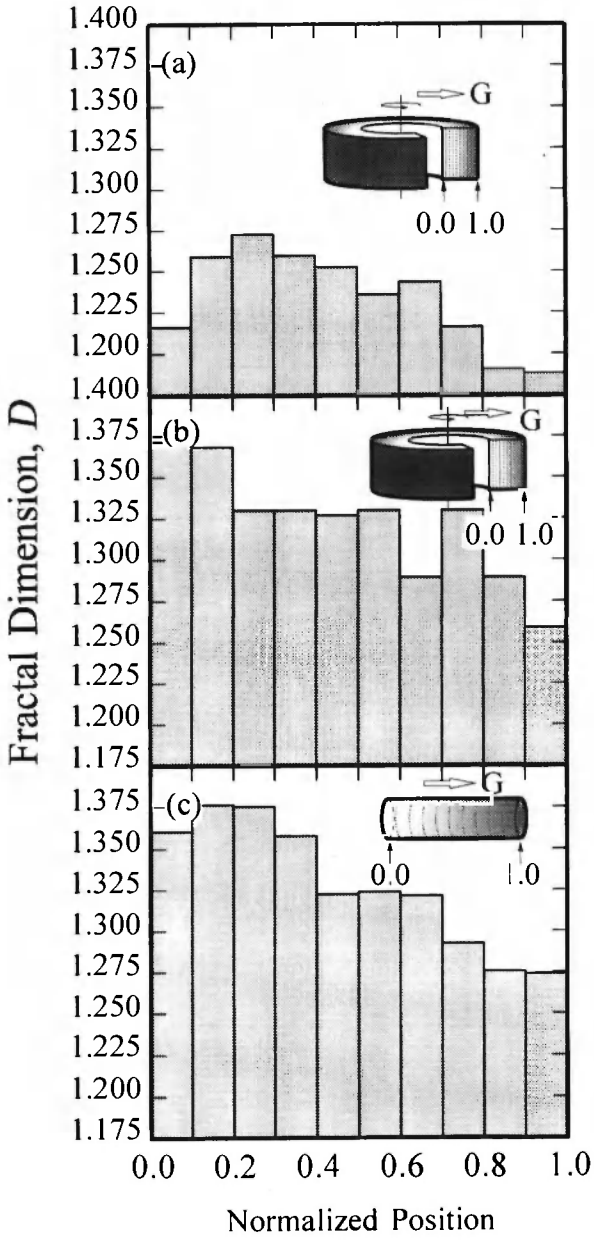

Fig. 11: Fractal dimension distributions of the Al_3Ni particles in the FGMs. (a), (b) and (c) are results of specimens R5, R7 and C1, respectively.

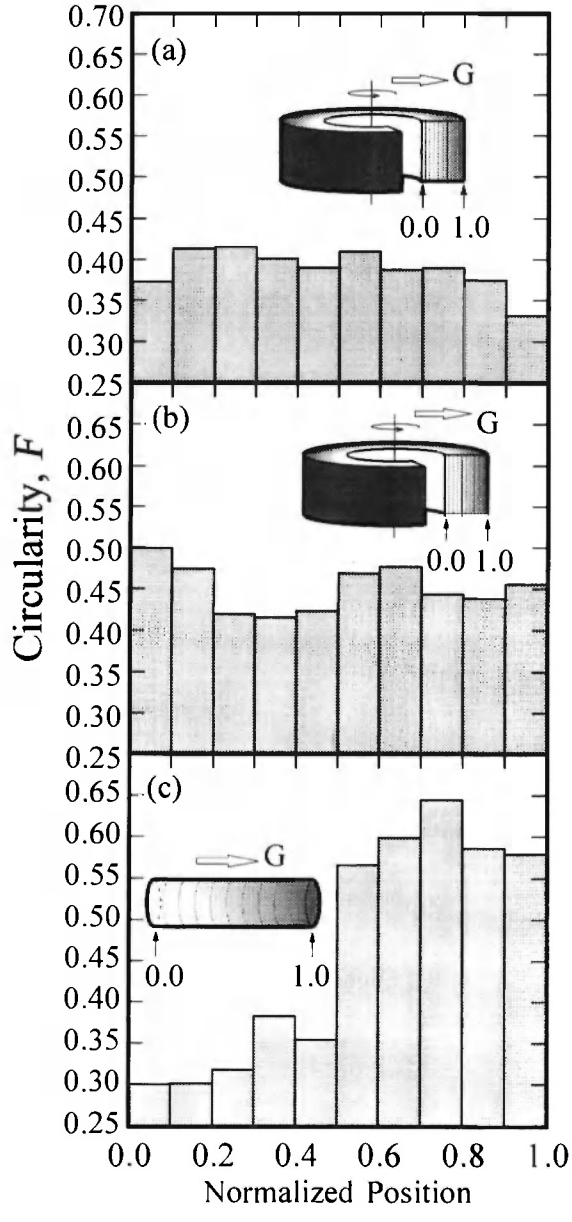

Fig. 12: Circularity distributions of the Al_3Ni particles in the FGMs. (a), (b) and (c) are results of specimens R5, R7 and C1, respectively.

that of smaller particles, the larger particles migrate faster than the smaller particles /4/. Consequently, the average particle size at the outer region of the ring is larger than that at the inner region. Such results conflict with the present results that the average particle size at the ring outer region is smaller than that at the inner region. In fact, since both the larger and smaller particles were identified to be Al_3Ni intermetallic compounds by EDX analysis, there is no density difference between the larger and smaller particles. Thus, the origin must be different in case of the FGMs fabricated by the centrifugal solid-particle method,

which can be explained according to the Stokes' law.

The next possibility is that the particle size may be influenced by local chemical composition based on the recent examination by Al-Cu system /11/. A process of the graded composition formation in the FGM fabricated by the centrifugal *in-situ* method under the centrifugal force has been discussed and it was concluded that a chemical composition gradient is formed before the crystallization of the primary crystal due to the density difference between co-existing atoms, *e.g.*, Al and Cu, in the liquid state. The primary crystals in the matrix appear depending on local chemical composition and migrate according to density difference, thus a further compositional gradient is formed. The above discussion is applied to the present Al-Ni system. Since the partial separation of Al and Ni in the liquid state occurs during the early stage of the centrifugal casting, the chemical composition of molten alloy at the ring outer region becomes Ni-rich before the crystallization of the Al_3Ni primary crystal. Then the crystallization can occur at higher temperature at the ring outer region because the initial master alloys are hyper-eutectic compositions, as shown in Figure 4. Consequently, the larger particles are formed at the outer part of the ring and *vice versa*. This conclusion also contradicts the present experimental results except that the particle sizes of the 13 mass% Ni specimens (specimens R1~R3) are smaller than those in the 20 mass% Ni specimens (specimens R4~R6), as shown in Figure 10. However, it is still impossible to explain why the smaller particle is formed at the ring outer region from a theory of the gradation of the chemical composition.

The third possibility is based on the well-known concept that the size of the crystallized particles is influenced by the solidification process. The temperature at the outer region of the ring is lower than that at the inner region in case of the centrifugal casting /18/. Therefore, the graded distribution of Al_3Ni primary crystal particles can be related to the difference in cooling rate within the ring. The cooling rate in this study is found to increase with G number as shown in Table 1. Then, the particle size at the ring outer region becomes smaller for the specimens fabricated under a larger G number, *i.e.*, faster cooling rate. Moreover, small gradients of particle size and larger average particle size are formed in the furnace-cooled specimens R7 and C1, in which the temperature gradient and cooling rate during solidification should be small. This means that the difference in the particle size distribution within the FGM fabricated by the centrifugal *in-situ* method can be caused by a difference in cooling rate.

5. 2 Origin of particle shape gradient

In the present study, the cylindrical specimen C1 shows the graded distribution of Al_3Ni particle shape arranged by both fractal dimension and circularity while the variation is not clear in the ring-shaped specimens. The ring-shaped specimens R5 and R7 were fabricated by the centrifugal *in-situ* method alone, while the fabrication method of specimen C1 belongs to both the centrifugal solid-particle and *in-situ* methods. However, particle shape should not be affected by the application of centrifugal force before the crystallization of Al_3Ni particles. Moreover, if the application of centrifugal force influences the Al_3Ni particle shape during the crystallization and the growth of Al_3Ni particles, particle shape of the ring-shaped specimens R5 and R7 might be different from that of the Al-Ni ingot. This hypothesis contradicts the experimental results. Therefore, the difference in the particle shape distributions may be caused by the difference in cooling rate or deformation of particles.

In order to examine the effect of cooling rate on particle shape, the fractal dimensions and circularities in furnace-cooled and air-cooled specimens fabricated without centrifugal force are calculated. The results are given in Table 2. There are no important differences between the furnace-cooled and air-cooled specimens. The particle shape is found to be distributed in the

Table 2

Fractal dimension and circularity values of furnace cooled and air cooled specimens fabricated under G = 1.

	Fractal dimension	Circularity
Furnace cooled specimen	1.20	0.44
Air cooled specimen	1.15	0.31

cylindrical specimen C1. Nevertheless, particle shape distribution has not appeared in the ring-shaped specimen R7 despite the same cooling rate having been applied. Judging from these results, the cooling rate effect alone may not explain the origin of particle shape gradient.

An alternative possibility is that the granular shape to ellipsoidal shape change takes place by stir effect /19/. To reveal the stir effect on the particle shape, an experiment under stirring was carried out. Representative microstructures at severely stirred regions of the stirred specimens are shown in Figure 13. It can be seen that the particle size decreases with increasing the stirring rate. Simultaneously, roundish particles are formed in the severely stirred specimen. Table 3 lists the fractal dimensions and circularities at severely stirred regions in the stirred specimens. It should be noted that a difference is found in the circularity values between Tables 2 and 3. The circularity increases by the stirring. Moreover, circularity increases with increasing the stirring rate. It had been reported that the roundish Al_3Ni particles are found in the semi-solid formed Al-Al_3Ni FGM /20/. Xia and Tausig have studied liquidus casting of an aluminum alloy 2618 (Al -2.3mass%Cu -1.6mass%Mg -1.1mass%Fe -1.0mass%Ni -0.18mass%Si -0.07massTi) for thixoforming. They found that the grains have been elongated along the flow direction /21/. Therefore, the present results agree well with the previous studies /20, 21/. In the case of the cylindrical specimen, severe stirring may occur around the top region, with a small stirring effect for ring-shaped specimens. The particle shape distributions in Figures 11 and 12 could be mainly realized in this way. We believe that, by detailed investigation of particle shape, we can obtain important information on the formation mechanism of composition gradient within the FGM fabricated by the centrifugal *in-situ* method.

Table 3
Fractal dimension and circularity values in the stirred specimens fabricated under $G = 1$.

	Fractal dimension	Circularity
250 rpm stirred specimen	1.29	0.57
500 rpm stirred specimen	1.28	0.64

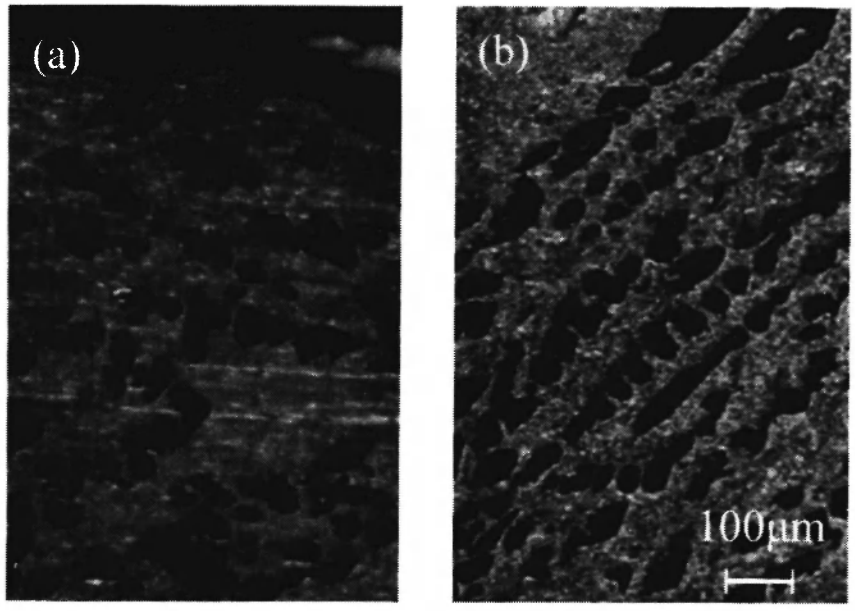

Fig. 13: Microstructures of stirred specimens at severely stirred regions at the rates of 250 rpm for (a) and 500 rpm for (b).

6. CONCLUSIONS

In this paper, we have carried out a microscopic study of the ring and cylindrical-shaped Al-Al_3Ni FGMs fabricated by a centrifugal *in-situ* method. The volume fraction, particle size, fractal dimension and circularity distributions within the FGMs are investigated through systematic centrifugal casting of two kinds of Al-Ni master alloys. The results are summarized as follows.

(1) The average three-dimensional diameter of Al_3Ni primary crystal particles within the *in-situ* Al-Al_3Ni FGMs varies gradually towards centrifugal force direction. Both volume fraction and particle size have graded distributions. The larger G number and the smaller initial Ni content in Al-Ni master alloy are results of a relatively small particle size. The particle size distribution within the FGM depended on the difference in cooling rate.

(2) Ring-shaped specimens show small graded variation of fractal dimension and almost constant circularity. In contrast, cylindrical FGM has larger graded variation concerning with fractal dimension and circularity gradients. Those characters are connected with the variation of particle shape and the origin of particle shape distribution is attributed to the stir effect rather than cooling rate difference. A notable position dependency of particle size and particle shape was found in the FGMs.

ACKNOWLEGEMENT

This work was supported by the Ministry of Education, Culture, Sports, Science and Technology of Japan, under the Grant-in-Aid for COE Research (10CE2003) and 21st Century COE Research.

REFERENCES

1. S. Surech and A. Mortensen, *Fundamentals of Functionally Graded Materials, Processing and Thermomechanical Behavior of Graded Metals and Metal-Ceramic Composites*, IOM Communications Ltd, London, 1998.
2. Y. Miyamoto, W.A. Kaysser, B.H. Rabin, A. Kawasaki and R.G. Ford, editor: *Functionally Graded Materials, Design, Processing and Applications*, Kluwer Academic Publishers, 1999.
3. Y. Fukui "Fundamental investigation of functionally graded material manufacturing system using centrifugal force" *JSME Int. J. Series III*, **34**, 144-148 (1991).
4. Y. Watanabe, N. Yamanaka and Y. Fukui "Control of composition gradient in a metal-ceramic functionally graded material manufactured by the centrifugal method" *Composites Part A*, **29A**, 595-601 (1998).
5. Y. Watanabe and Y. Fukui "Microstructures and mechanical properties of functionally graded materials fabricated by a centrifugal method" *Rec. Res. Devel. Metall. Mater. Sci.*, **4**, 51-93 (2000).
6. Y. Fukui and Y. Watanabe "Analysis of thermal residual stress in a thick-walled ring of duralcan-base Al-SiC functionally graded material" *Metall. Mater. Trans. A*, **27A**, 4145-4151 (1996).
7. Y. Watanabe, H. Eryu and K. Matsuura "Evaluation of three-dimensional orientation of Al_3Ti platelet in Al-based functionally graded materials fabricated by a centrifugal casting technique" *Acta Mater.*, **49**, 775-783 (2001).
8. Y. Watanabe, A. Kawamoto and K. Matsuda "Particle size distribution in functionally graded materials fabricated by the centrifugal solid-particle method" *Comp. Sci. Tech.*, **62**, 881-888 (2002).
9. T. W. Clyne and P. J. Whithers, *An Introduction to Metal Matrix Composites*, Cambridge University Press, Cambridge, p.344, 1993.
10. Y. Fukui, K. Takashima and C. B. Ponton, "Measurement of Young's modulus and internal friction of an *in situ* Al-Al_3Ni functionally gradient material" *J. Mater. Sci.*, **29**, 2281-2288 (1994).
11. S. Oike and Y. Watanabe "Development of *in-situ* Al-Al2Cu functionally graded materials by a centrifugal method" *Inter. J. Mater. Prod. Tech.*, **16**, 40-49 (2001).
12. Y. Oya-Seimiya, T. Shinoda and Y. Watanabe "Optimization of the *in-situ* Al-Si base functionally graded material fabricated by

centrifugal casting" *Mat. Res. Soc. Symp. Proc.*, **707**, 333-338 (2002).

13. M. Tanaka, A. Kayama and R. Kato "Fractal nature of fracture surfaces and microstructures in materials," *Rec. Res. Devel. Metall. Mater. Sci.*, **4**, 1-33 (2000).
14. T. B. Massalski, Editor-in-Chief: *Binary Alloy Phase Diagrams, Second Edition Plus Updates on CD-ROM* Version 1.0 (ASM International, USA 1996).
15. Y. Fukui, N. Yamanaka, Y. Watanabe and Y. Oya-Seimiya, "Fabrication of in-situ Al-Al_3Ni functionally graded material by centrifugal method," *J. Jpn Light Met.*, **44**, 622-627 (1994). (in Japanese)
16. R. T. DeHoff, "Measurement of number and average size in volume"; pp. 128-148 in *Quantitative Microscopy*, Edited by R. T. DeHoff, F. N. Rhines. McGraw-Hill Book Company, New York, 1968.
17. K. Matsuda, Y. Watanabe, M. Kamijo and Y. Fukui, "Evaluation of particle-shape graded materials by fractal analysis," *Functionally Graded Materials 2001*, 125-130 (2002). (in Japanese)
18. C. G. Kang and P. K. Rohatgi, "Transient thermal analysis of solidification in a centrifugal casting for composite materials containing particle segregation," *Metall. Mater. Trans. B*, **27B**, 277-285 (1996).
19. K. Miwa, G. Yoshinari and T. Ohashi, "Changes in eutectic structure and apparent viscosity by stirred of solidification Al-Al_3Ni near eutectic alloys," *J. Jpn Inst. Metals.*, **49**, 483-489 (1985). (in Japanese)
20. Y. Fukui, H. Okada, N. Kumazawa and Y. Watanabe, "Near net shape forming of Al-Al3Ni FGM over eutectic melting temperature," *Metall. Mater. Trans. A*, **31A**, 2627-2636 (2000).
21. K. Xia and G. Tausing, "Liquidus casting of a wrought aluminum alloy 2618 for thixoforming", *Mater. Sci. Eng. A*, **246**, 1-10 (1998).